INJURY BIOMECHANICS RESEARCH
Proceedings of the Thirty-Seventh International Workshop

Assessment and Validation of a Methodology for Measuring Anatomical Kinematics During Impact Loading

D.J. Lessley, S.V. Purtsezov, C.G. Shaw, D.P. Parent, P.O. Riley, R.W. Kent and J. R. Crandall

ABSTRACT

Video-based optoelectronic stereophotogrammetric systems (OSSs) have recently been employed for kinematic measurement during impact tests with post mortem human surrogates (PMHSs). Application of this methodology requires specialized target hardware to be attached to anatomical structures of interest (e.g. individual ribs, vertebrae, head, pelvis, and shoulders). The hardware supports retroreflective spherical targets which are visible to the OSS. The recorded target motion is then transformed to the underlying anatomical structures to quantify the trajectories of individual bones throughout the impact event. This study presents the results of seven tests that were conducted to practically assess the efficacy of this emerging methodology for measuring anatomical kinematics during impact loading. A single dynamic test used an 8-camera 1000 Hz Vicon MX^{TM} motion capture system and rigid structure to assess intrinsic optical error associated with the OSS, and also to evaluate the ability of the rigid body motion analysis to reproduce directly measured anatomical motion using remotely collected target data. The remaining six tests were conducted to assess the effect of compliance in the assumed rigid connection between the visible target hardware and underlying bone on the transformed displacements at a desired anatomical location (e.g. the center of a rib). A rigid test fixture was constructed to support a non-yielding 18 mm diameter steel rod simulating a segment of an anterior rib (rib). A retroreflective four-target cluster was then attached to the rib using the same hardware employed to optically measure anterior ribcage displacement in frontal sled tests with restrained PMHSs. During the tests a 16-camera 1000 Hz Vicon MX^{TM} motion capture system was used to optically track the cluster motion which was then transformed to the center of the rib segment. Deviation between the transformed rib center and the actual rib center was determined for each test. In four of the tests the cluster was loaded laterally to its support structure using either 22.5 N or 43 N to simulate *inertial loads acting on the structure under impact conditions. Two additional tests forced rotation between the cluster mounting hardware and the simulated rib. The results demonstrate robust performance of a novel methodology combining state-of-the-art optical technology and rigid body motion analysis to obtain kinematic measurement of anatomical structures within the human body which are not visible for direct measurement.*

INTRODUCTION

For the field of injury biomechanics the importance of accurately quantifying how the human body moves and deforms during an impact is paramount. In order to improve the current understanding of human kinematic response to impact loading it is necessary to obtain a detailed knowledge of how individual structures within the body move (e.g. individual bones such as vertebrae and ribs). Accurately quantifying the motion of such anatomical structures during an impact event is a difficult yet essential task in effectively characterizing human kinematic response, and is necessary for quantifying injury risk and developing optimal countermeasures for human protection. Accomplishing this goal, however, requires improved methods for measuring these vital kinematic responses during impact loading events.

Kinematic measurements during high-rate events such as impact testing have historically been accomplished using two-dimensional (2D) video analysis from conventional high-speed video imaging (Forman et al., 2006 and 2009) and are illustrated in Figure 1. Using this technique the trajectory of a visible photo target on the surface of the body is tracked relative to either the vehicle or a fixed laboratory reference frame. This method, however, is confounded by several factors 1) the fact that the anatomical structure of interest is within the body and not directly visible to the high-speed imager 2) the actual 3D motion of such an anatomical structure is approximated by the 2D motion of the overlying photo target and 3) such analysis is limited by the issues of imager lens distortion and parallax. While such analysis has long been the standard for kinematic analysis in the field of impact biomechanics, the associated limitations prevent a comprehensive kinematic analysis to be performed that includes the 3D motion of individuals bones and deformation of the torso (Lopez et al,. 2009).

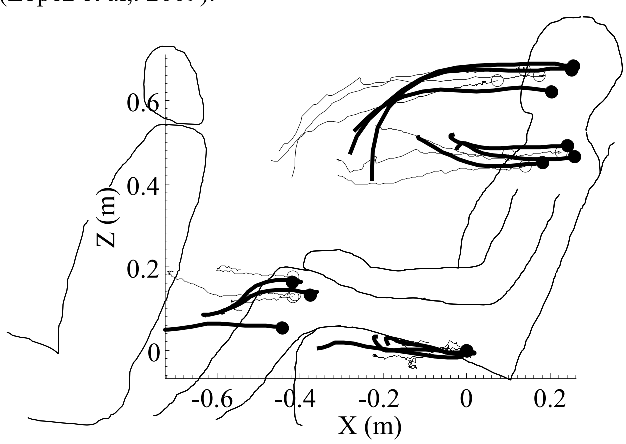

Figure 1: Conventional high-speed imaging kinematic analysis results from impact tests involving PMHS (from Forman et al. (2009)).

Recently, in the field of impact biomechanics, high-rate video-based optoelectronic stereophotogrammetric systems (OSSs) (Figure 2) have been employed using a specialized methodology to provide kinematic measurement of anatomical structures using a rigid body motion analysis (Shaw et al., 2007, Lessley et al., 2008 and 2009, and Shaw et al., 2009). The optical system tracks the displacements of visible four-target clusters (clusters) rigidly attached to a corresponding underlying bone during impact tests using post mortem human surrogates (PMHSs) as illustrated in Figure 3. The collected cluster trajectory is then transformed to the bone (Figure 4) to provide the motion of structures (bones) that are within the body and which are not directly visible to the optical system such as individual ribs and vertebrae. The details of the utilized rigid body motion analysis and associated coordinate transformation are provided in the Appendix.

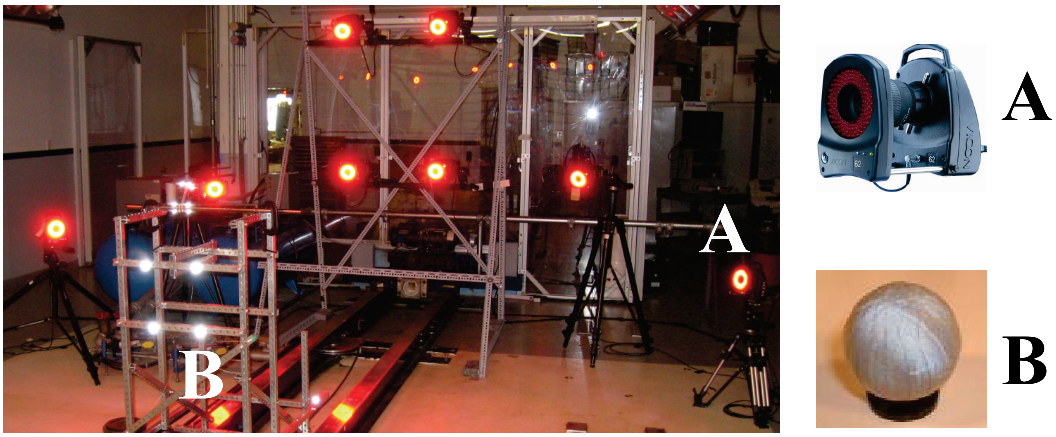

Figure 2: 16-camera optoelectronic stereophotogrammetric system (OSS) and retroreflective targets (B). Only 8 of the 16 cameras (A) are shown here.

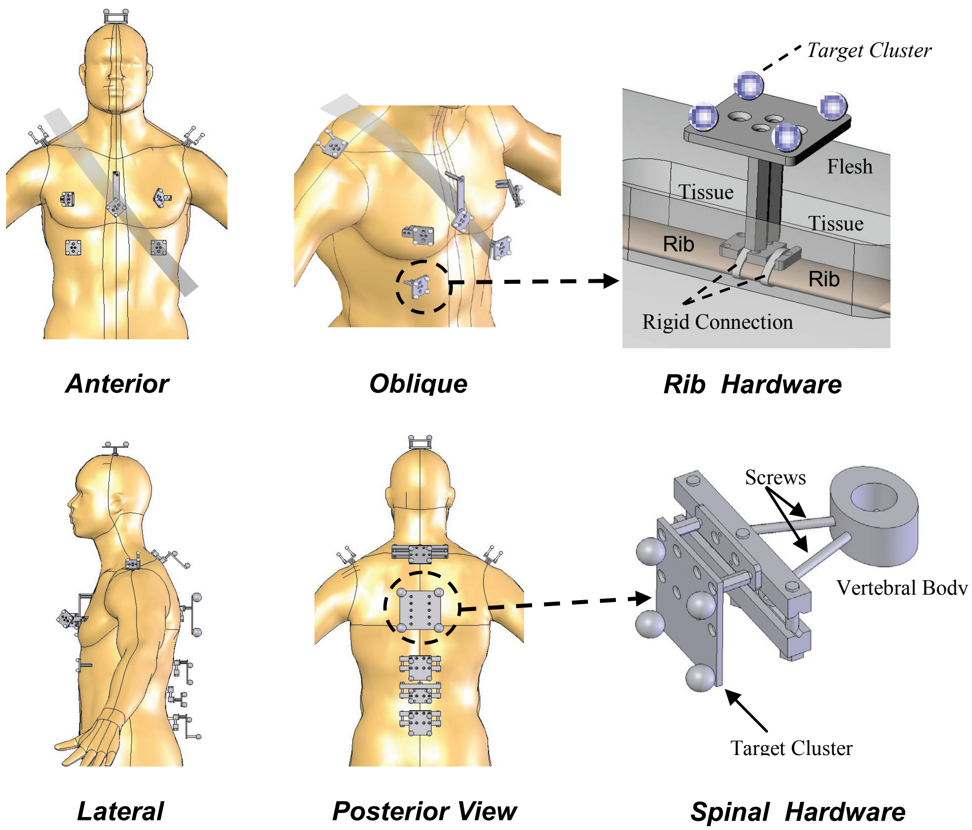

Figure 3: Kinematic measurement hardware. Hardware supporting retroreflective target clusters are rigidly fastened to various structures of interest within the body (e.g. ribs, vertebrae, shoulders, head, and pelvis). Collected optical trajectory data from the visible target clusters is then transformed to the corresponding bones to provide trajectories of individual bones (see Figure 4 and Appendix)(adapted from Shaw et al. (2009)).

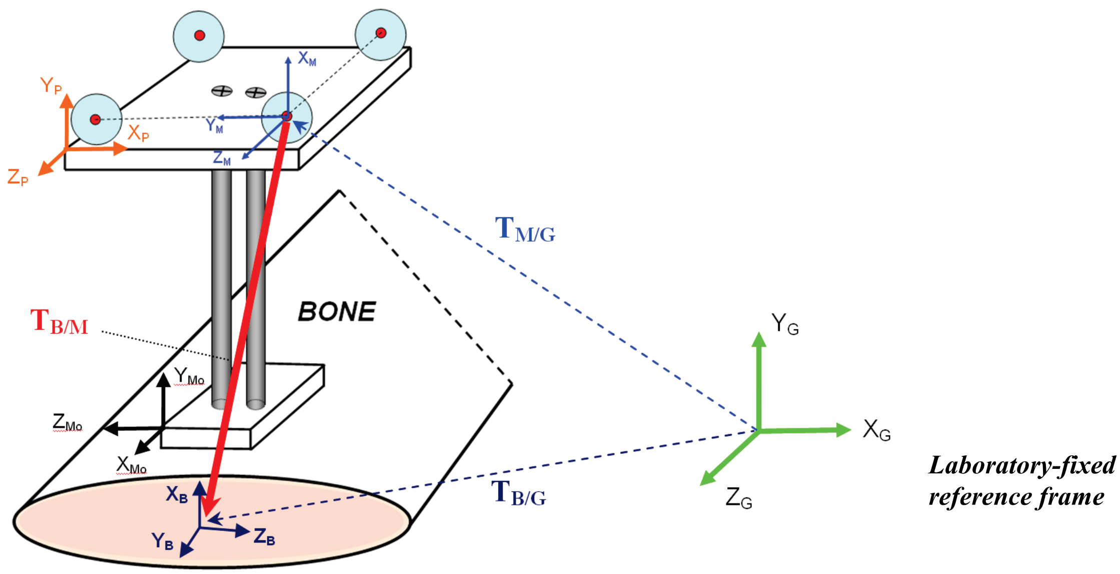

Figure 4: Rigid body motion analysis. At a given location, hardware supporting a retroreflective target cluster is rigidly fastened to the bone of interest. The trajectory of the visible target cluster is then transformed to the bone using a coordinate transformation. See Appendix for coordinate transformation details.

The introduction of video-based optoelectronic stereophotogrammetry for PMHS impact loading is relatively recent, however, it has long been utilized in non-impact motion biomechanics applications such clinical gait analysis (Cappozzo et al., 2010). The objective in movement analysis is the reconstruction of anatomical motion in the global OSS reference frame (Figure 4), however, it is generally accepted that a primary limitation of stereophotogrammetry movement analysis is error in single target position data and the propagation of this error to the estimation of the desired anatomical motion (Chiari et al., 2005 and Cappozzo et al., 2010). Considerable effort has been made to quantify and reduce instrumental errors as well as to set forth experimental guidelines regarding estimating anatomical motion from remotely placed targets (Chiari et al., 2005 and Cappozzo et al., 1995). While entire studies have been devoted to quantifying performance of commercially available OSSs (Ehara et al. 1995, Ehara et al. 1997, Klein et al. 1995, Linden et al., 1992, Haggard et al., 1990, Thornton et al. 1998, and Richards, 1999), the variations in performance and technology coupled with sensitivity to OSS configuration warrants essential ad hoc investigations or “spot checks” to quantify the performance for a specific experimental configuration (Della Croce and Coppozzo, 2000 and DeLuzio et al., 1993). This is especially true for the impact loading environment where little or no performance data exists for the much higher loading and capture rates.

Throughout the development of the presented methodology for measuring anatomical motion during impact loading, an ongoing concern and design consideration has been that the combination of OSS error and unintended compliance in the cluster-to-bone connection could lead to unreasonable uncertainty in the calculated anatomical trajectories. The accuracy of the final anatomical trajectory depends on three major factors 1) the magnitude of intrinsic optical error in data collected from the OSS 2) the propagation of this intrinsic optical error to the anatomical location through the coordinate transformatoin and 3) the effect of compliance in the assumed rigid connection between the visible target clusters and underlying bone. This study presents the results of eight tests that were conducted to practically assess the efficacy of an emerging methodology for measuring anatomical kinematics during impact loading. The objective of this study is threefold which, specifically, is 1) to evaluate the quality of single target data collected from a basic OSS configuration used during impact conditions 2) to demonstrate the ability of the rigid body motion analysis to use remotely measured data to reproduce a known trajectory and 3) to comprehensively assess the effect of compliance in the assumed rigid connection between the target cluster and bone on the transformed trajectory of a desired anatomical location (e.g. the center of a rib). The combined errors will provide an estimate of the general magnitude of uncertainty with which anatomical motion can currently be measured during impact loading.

.

METHODS

Single target data quality and rigid body motion assessment

A dynamic test was conducted using the rigid cluster-rib composite illustrated in Figure 5 to assess 1) single target data quality and 2) the ability of the of the rigid body motion analysis to reproduce a directly measured trajectory using remotely measured cluster data. The rigid composite (Figure 5) was manually driven over a 0.635m trajectory at approximately 5 m/s. An 8-camera OSS configuration similar to that illustrated in Figure 2 captured the target trajectories at 1000Hz during the test. Prior to the test the OSS was calibrated (Zhaug, 1995, Cerveri et al., 1998, and Borghese et al., 2001) using a manufacturer supplied software based algorithm (Vicon IQ 2.5) such that the root mean squared error was < 0.4 mm over the capture volume.

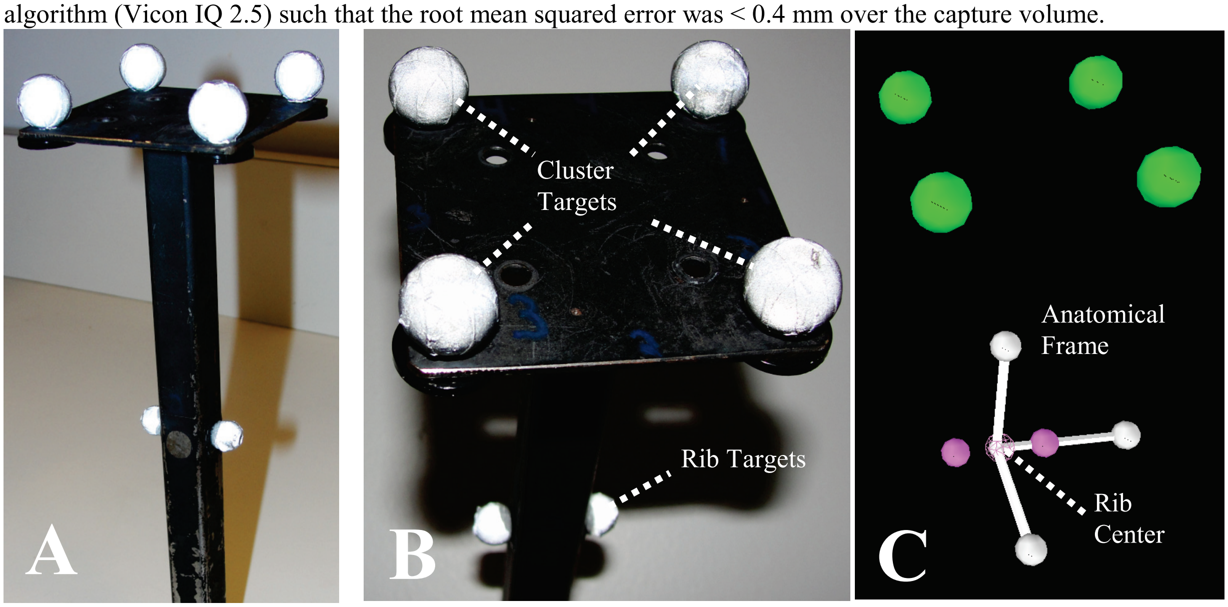

Figure 5: Rigid cluster-rib composite (A) outfitted with cluster targets (B) and rib targets (B). During the test the cluster data was transformed to the desired anatomical location which was the rib center and was defined to be the mean position of the two rib targets (B). Processed 3D position of all targets and transformed anatomical coordinate frame (C).

Rigid Body Motion Assessment. The composite structure was used to rigidly connect the cluster targets to a simulated anatomical location, referred to here as the "rib". During an actual PMHS impact test, the anatomical location of interest (e.g. a rib) is within the body and hidden from view and must be determined from the cluster motion. Here, however, both the cluster and rib motions were able to be directly tracked during the same dynamic event. The collected cluster data was used as an input in a motion analysis to obtain a calculated (i.e. transformed) anatomical trajectory to be compared with the directly measured anatomical trajectory. Specifically, referring to Figure 5, collected cluster target data (B) were transformed to the rib center (C) which was taken to be the mean of the rib target (B) positions. Comparison of the "transformed" anatomical trajectory with the directly measured anatomical (i.e."rib") trajectory provided a practical verification and quality assessment of rigid body motion analysis.

Single Target Data Quality Assessment Tests. Prior to the test described above the composite was digitized using a FARO arm (model N10). The digitized 3D points were used to create a high-quality digital representation of the target cluster to be compared with single target data collected during the test as illustrated in Figure 6. For each frame of collected data, the center positions of the four targets from the digital representation were optimally fit to the collected single target data using a least squares pose (LSP) optimization (Arun et al., 1987, Beldpans et al., 1988, Magnani et al., 1993, Soderkvist and Wedin, 1993, Wang et al., 1993, Cappello et al., 1994, Challis, 1995, Cappello et al., 1996, and Cappozzo et al., 1997) as illustrated in Figure 6. Deviations, $\delta_i(t)$, between the digital representation and the collected target data provided measures of single target error for the four targets comprising the cluster. Additionally the known diagonal distances between targets on the cluster for each optical frame were compared with those of the digital representation (Equations 1 and 2) as an alternate measure of single target error (Della Croce and Cappozzo, 2000, Cappozzo et al., 1993 and 1997, Morris and Mac Leod, 1990, Ehara et al., 1995 and 1997, and Holden et al., 2003).

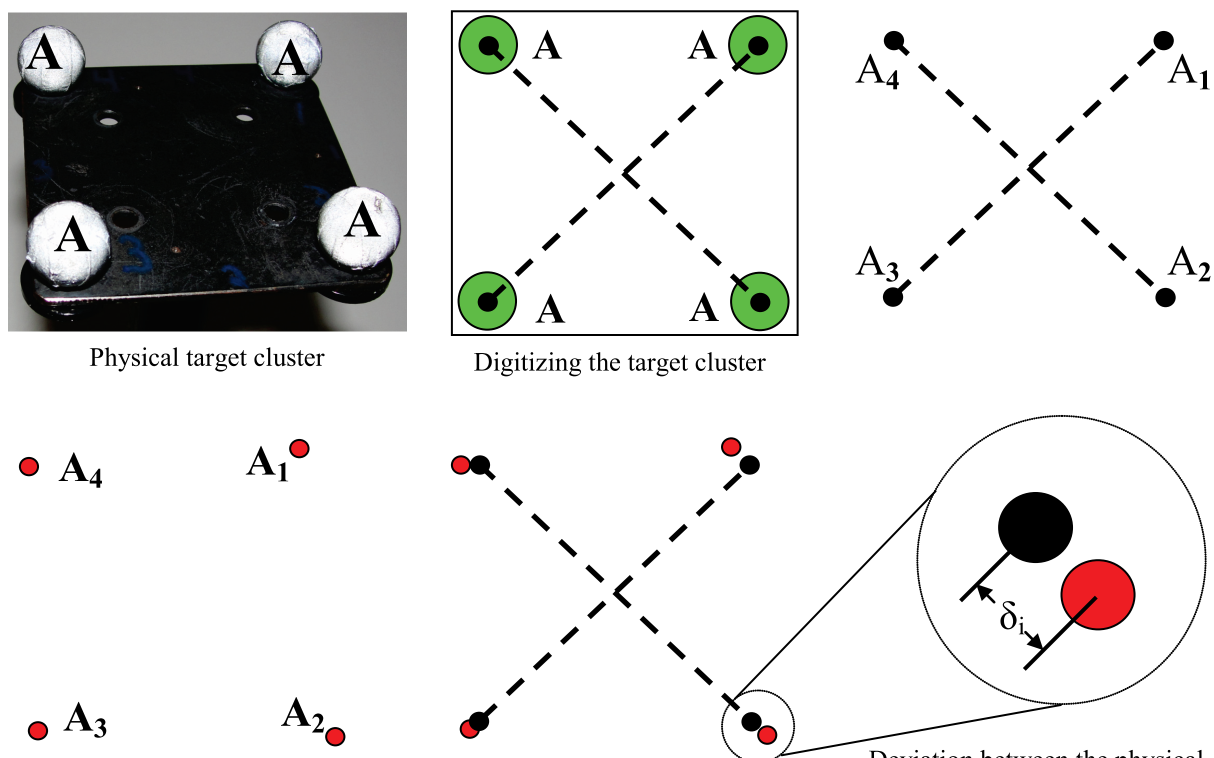

Physical target cluster

Digitizing the target cluster

Single target cluster positions for a single frame from the OSS

Application of the LSP estimator (Cappozzo et al. 1997) to optimally fit the digital representation to the single target data

Deviation between the physical representation and the corresponding single target data for a single collected optical frame during the dynamic event.

Figure 6: Single target data quality assessment. The physical target cluster was digitized to create a digital representation of the target cluster and was compared with the collected data from a dynamic test to quantify the magnitude of error associated with the OSS.

$$\Delta_{Diag_1}(t) = \overline{A_1 A_3}_{Optical}(t) - \overline{A_1 A_3}_{Digital\_representation} \quad [1]$$

$$\Delta_{Diag_2}(t) = \overline{A_2 A_4}_{Optical}(t) - \overline{A_2 A_4}_{Digital\_representation} \quad [2]$$

Hardware compliance assessment

In conjunction with the OSS kinematic measurement methodology, a range of specialized hardware configurations are utilized for PMHS tests to support retroreflective target clusters (Shaw et al., 2009). Of these hardware configurations, the greatest potential for compliance exists at the anterior ribcage measurement locations which require hardware that is strapped to the rib rather than screwed to prevent stress concentrations that could lead to fracture. Thus, the anterior ribcage hardware was considered a worst case and was selected to serve as the tested hardware for each of these reported tests.

Test Fixture and Setup. A rigid test fixture was constructed to support a non-yielding 18 mm diameter steel rod simulating a segment of an anterior rib (rib). A cluster was then attached to the rib using a representative range of hardware configurations employed to optically measure anterior ribcage displacement in frontal sled tests with restrained PMHS (Figure 3). Specifically, two hardware configurations were used (standard and modified) and are illustrated in Figure 7. Each configuration was rigidly attached to the rib using the same high-strength nylon straps used to attach the hardware to the rib in PMHS tests. A 16 camera 1000 Hz Vicon MX^{TM} OSS and camera configuration used for PMHS sled tests reported by Shaw et al. (2009) was used to track the cluster motion (refer to Figure 2). In addition to the cluster, four additional markers were symmetrically attached directly to the rib surface. The mean position of these four rib surface makers was taken to be the center of the rib which was also the target anatomical location for the cluster data to be transformed to (Figure 7).


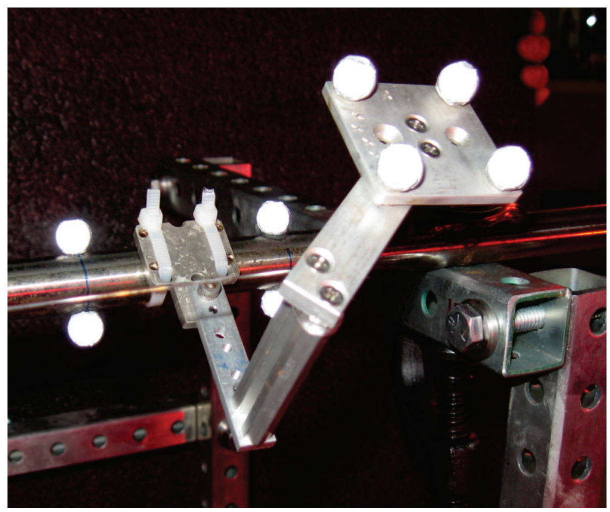

Figure 7: Test set up. Two hardware configurations, standard (left) and modified (right) were rigidly attached to the rib using high-strength nylon straps. These hardware configurations are representative of the range used in recent PMHS sled tests.

Test Condition. The test conditions selected for the assessment tests were based on the two most likely modes of hardware compliance which were considered to be 1) rotation around the rib and 2) bending due to inertial loading during the impact event. The rotational and bending compliance assessment tests are illustrated in Figure 8. For the rotational tests the hardware was driven through an angle of approximately 100 degrees using a manually tensioned nylon cable connected just beneath the target cluster, however only the initial 20 degrees of rotation were selected for analysis based on maximum rotation estimates from the PMHS tests. For the bending compliance tests, the simulated inertial load, $\mathbf{F}_{Applied}$, was nominally either 22.5 N or 43 N for a given test. $\mathbf{F}_{Applied}$ was generated using a weight that was slowly released to tension a cable attached just beneath the cluster which applied a force perpendicular to the cluster supports. The selected values for $\mathbf{F}_{Applied}$ are based on estimates of inertial loading from conducted PMHS sled tests. 22.5 N was selected using the product of the maximum resultant sternal acceleration and the maximum hardware mass (56.5 grams), and is considered a reasonable worst case. 43 N was selected for duplicate tests to evaluate the effect of doubling the initial worst case estimate. A detailed summary of all conducted tests and conditions is provided in Table 1.

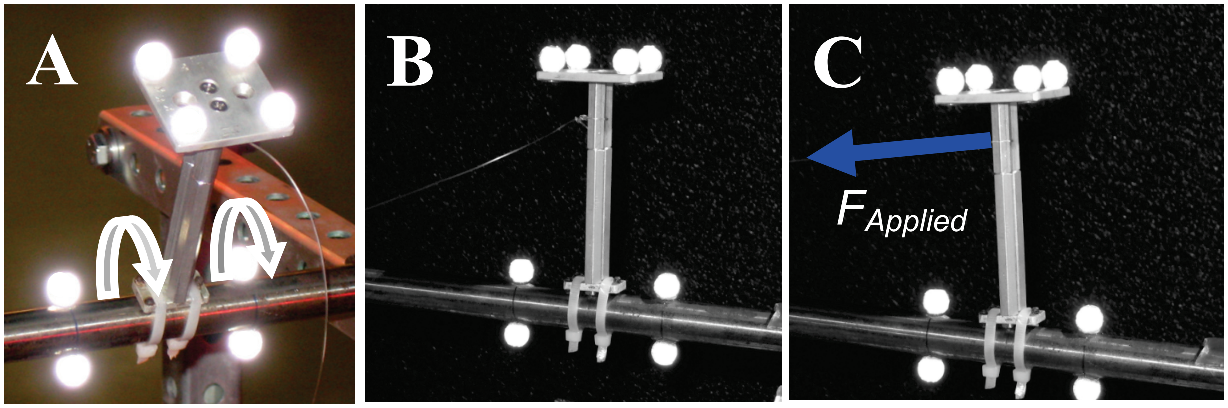

Figure 8: Bending and rotational compliance assessment. (A) illustrates the rotational compliance assessment, while (B) and (C) illustrate the bending compliance assessment test. (B) illustrates the hardware prior to loading and (C) illustrates the hardware under the simulated inertial load, $\mathbf{F}_{applied}$.

Data Processing and Compliance Error Assessment. For each test optical target data was collected by the 16-camera Vicon OSS at 1000Hz. During post-processing each frame of collected cluster data was transformed to the center of the rib using the methods provided in the Appendix. From here on, the cluster data that is transformed to the center of the rib will be referred to as the "*transformed rib center* ". The mean position of the four targets symmetrically fixed to the rib marked the actual center of the rib, which will be referred to from here on as the "*actual rib center*". At the start of the test the position of transformed rib center was coincident with the actual rib center, however, induced rotation or deformation of the hardware caused the transformed rib center position to deviate from the actual rib center position. This deviation, Δ_{Trans}, between transformed rib center and actual rib center was taken as the magnitude of the error due to hardware compliance. Δ_{Trans}, illustrated in Figure 9, is calculated for all tests using Equation 3. Figure 10 provides the initial configuration, at T_{zero}, for a given test using a side-by-side comparison of the physical setup with the processed 3D results illustrating the positions of all targets, transformed rib center, and actual rib center. It should be noted (referring to Figure 10) that the transformed rib center is the origin of the orthogonal coordinate system created during the rigid body motion analysis and illustrated in Figure 10 (refer to Appendix for additional details regarding the rigid body motion analysis).

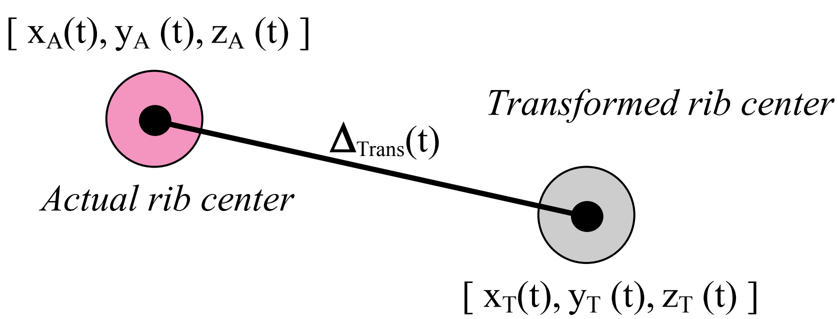

Figure 9. Deviation, Δ_{Trans}, due to hardware compliance.

$$\Delta_{Trans}(t) = \sqrt{(x_T(t) - x_A(t))^2 + (y_T(t) - y_A(t))^2 + (z_T(t) - z_A(t))^2} \quad , \quad \text{where } \Delta(0) = 0 \qquad [3]$$

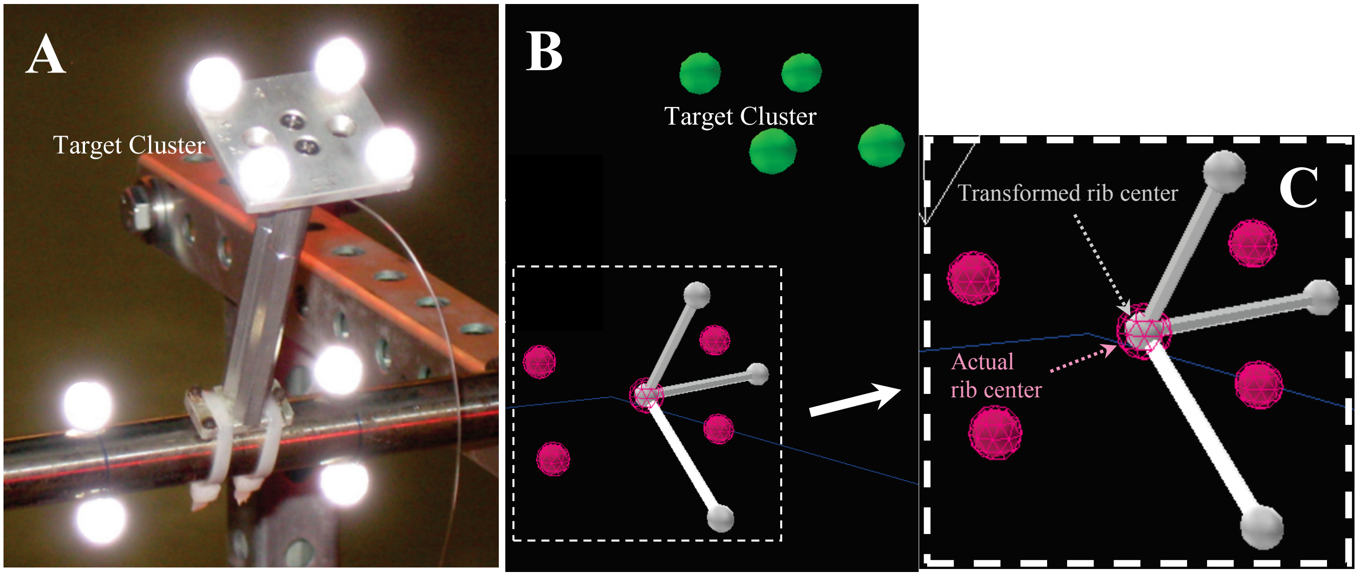

Figure 10: (A) the initial configuration at T_{zero}. (B) Processed 3D position of all targets and transformed rib center coordinate system at T_{zero} corresponding to the initial configuration show in (A). (C) Illustration of the transformed rib center and actual rib center referred to in Figure 9 and Equation 3. The transformed rib center is the origin of the orthogonal coordinate system created during the rigid body motion analysis illustrated in (C).

Summary of conducted assessment tests

Details concerning all conducted tests for this study are provided below in Table 1.

Table 1. Test Matrix and Summary of Conducted Tests

TEST #	Assessment Test Description	Hardware Description	Rate	$F_{Applied}$	Cluster Dimensions	Cluster-to-Transformation Target Distance†	Refer to Figures
001	Single Target Data Quality	Composite	Dynamic	NA	51 mm x 51 mm	105.9 mm	5 and 6
002	Rotational	Standard	Dynamic	NA	29 mm x 29 mm	95.4 mm	7 and 8
003	Bending	Standard	Quasi-Static	22 N	29 mm x 29 mm	95.4 mm	7 and 8
004	Bending	Standard	Quasi-Static	44.5 N	29 mm x 29 mm	95.4 mm	7 and 8
005	Rotational	Modified	Dynamic	NA	29 mm x 29 mm	89.3 mm	7 and 8
006	Bending	Modified	Quasi-Static	22 N	29 mm x 29 mm	89.3 mm	7 and 8
007	Bending	Modified	Quasi-Static	44.5 N	29 mm x 29 mm	89.3 mm	7 and 8

† -- Distance from cluster center to target location of the transformation (i.e. magnitude of position vector associated with cluster coordinate system transformation)

RESULTS

Seven tests were successfully conducted with a Vicon manufactured OSS using a range of anatomical measurement hardware configurations and test conditions. The OSS single target position error assessment (Test 001) resulted in average deviations, δ_i, of 0.2 mm, 0.5 mm, 0.4 mm, and 0.3 mm for the composite cluster targets 1 - 4 respectively over the duration of the dynamic event, while peak deviations, δ_i, were 0.5 mm, 0.9 mm, 0.8 mm, and 0.6 mm for the composite cluster targets 1 - 4 respectively. In addition, mean values for diagonal distance deviation, Δ_{Diag}, ranged from 0.3 mm to 0.5 mm with peak values ranging from 0.6 mm to 1.1 mm. A summary of results for single target position data quality is provided below in Table 2 and Figure 11. Refer to Figure 6 and Equations 1 and 2. Results of the rigid body motion assessment (Test 001) are illustrated in Figure 12 providing comparison of trajectories of the cluster, rib, and transformed cluster data to the rib (transformed).

Table 2. Summary of Single Target Position Error†

Test #	δ_1	δ_2	δ_3	δ_4	Δ_{Diag1}	Δ_{Diag2}
Max	0.5	0.9	0.8	0.6	0.6	1.1
Mean	0.2	0.5	0.4	0.3	0.3	0.5
S.D	0.1	0.1	0.1	0.1	0.1	0.1

† -- All values in mm.

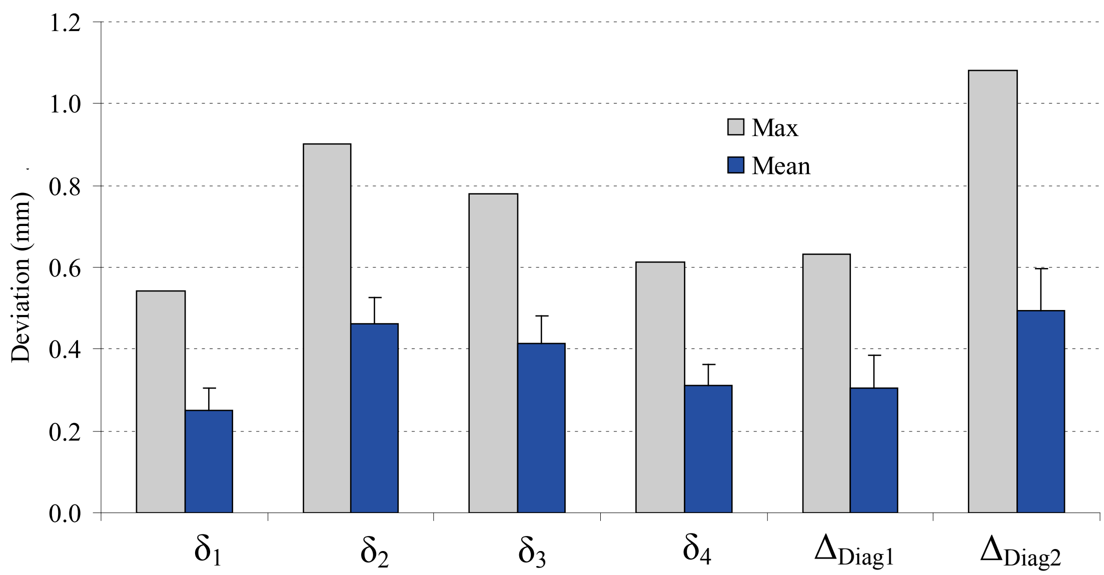

Figure 11: Summary of single target position error.

Rotational compliance tests (Test 002 and 005) resulted in transformation deviations, Δ_{Trans}, of 1.7 mm and 0.9 mm for the standard and modified hardware configurations respectively. Bending compliance tests with the standard hardware (Test 003 and 004) resulted in transformation deviations, Δ_{Trans}, of 1.1 mm and 1.6 mm for the 22 N and 44.5 N tests respectively. Bending compliance tests with the modified hardware (Test 006 and 007) resulted in transformation deviations of 0.9 mm and 1.1 mm for the 22 N and 44.5 N tests respectively. A summary of the Δ_{Trans} results for all tests is provided below in Table 3 and Figure 13. Additionally, time histories of Δ_{Trans} and resultant cluster displacement for all tests are provided in Figure 14.

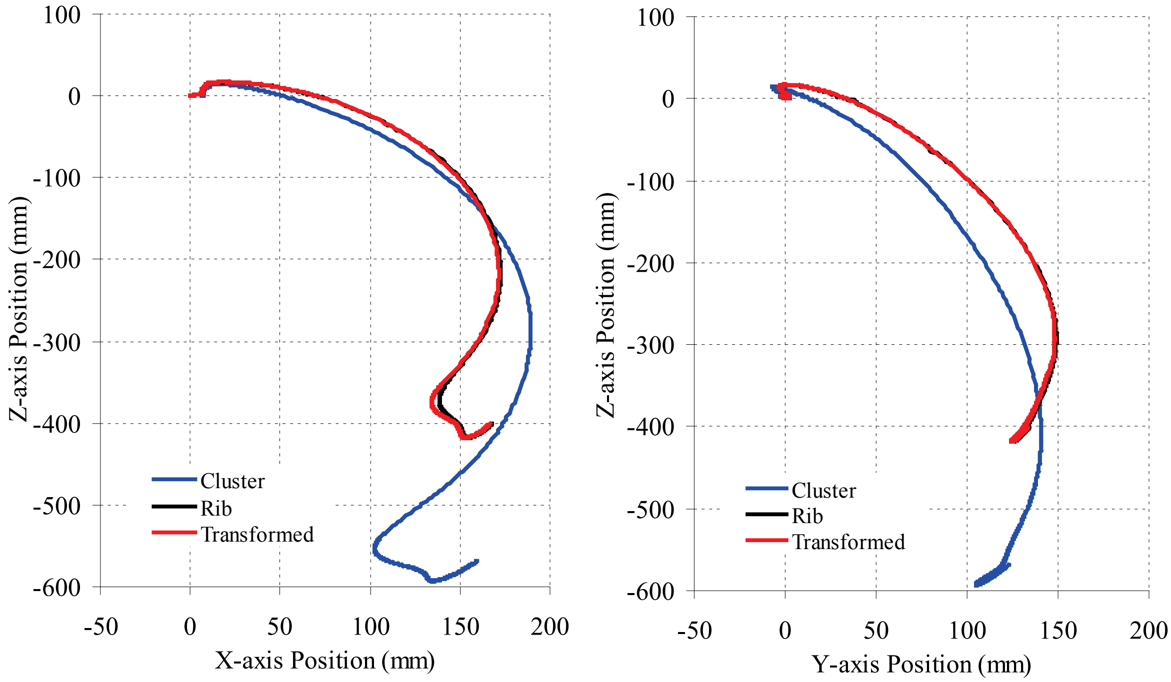

Figure 12: Rigid body motion assessment results (Test 001). Views of the trajectories in both the Z-X and Z-Y planes. Cluster and rib trajectories were obtained directly from the OSS. Remotely measured cluster data was transformed to the rib to obtain the "Transformed" trajectory.

Table 3. Summary of $\Delta_{Trans}(t)$ Results from all Tests.

Test #	**001**	**002**	**003**	**004**	**005**	**006**	**007**
Max†	4.3	1.7	1.1	1.6	0.9	0.9	1.1
Mean†	0.3	0.3	0.4	0.7	0.4	0.3	0.5
S.D†	0.6	0.4	0.2	0.3	0.2	0.1	0.2

† -- All values in mm.

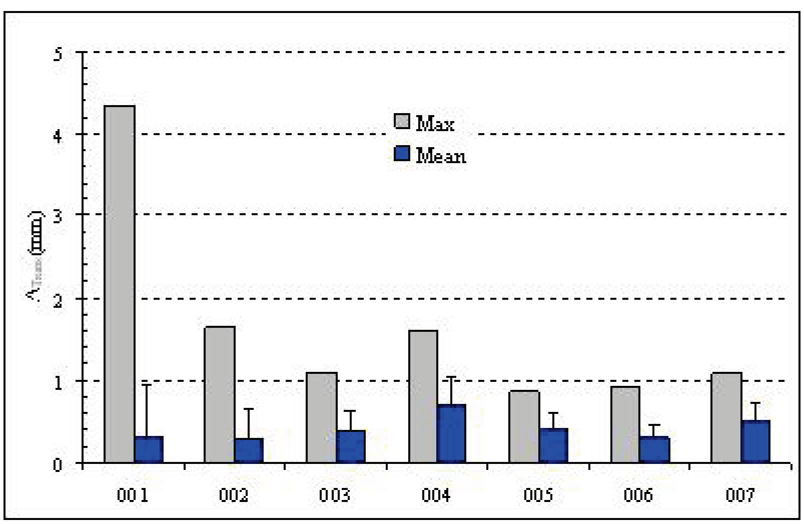

Figure 13: Summary of results for Δ_{Trans} from all tests.

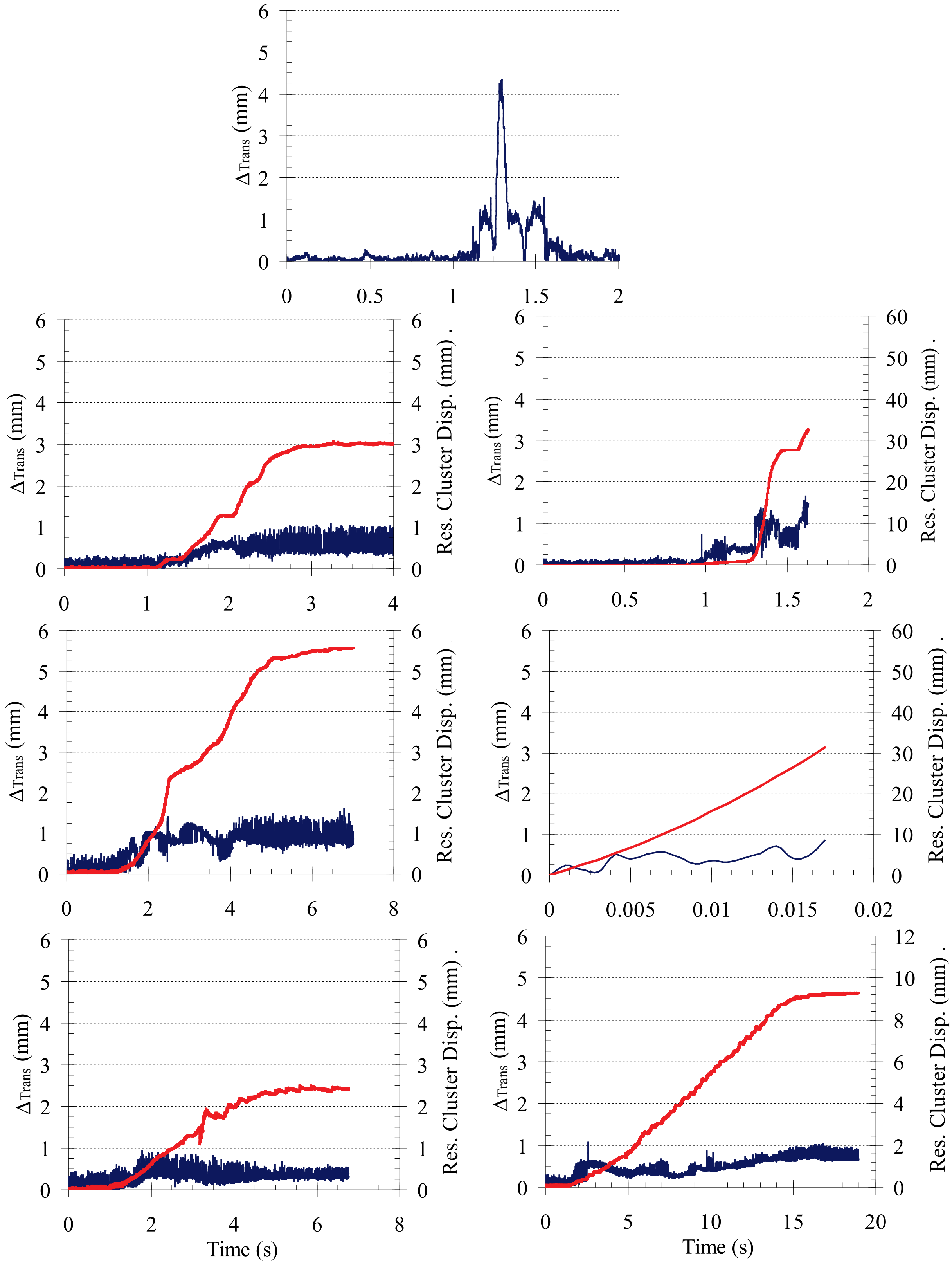

Figure 14: Time-history traces of Δ_{Trans} and resultant cluster displacement for all tests.

DISCUSSION

Applications for detailed kinematic data ranges from the development of advanced restraint systems to improving existing crash test dummies. Kinematic response also plays a foundational role in the development of improved computational models which are powerful tools for developing optimal countermeasures, however, the efficacy of such tools is highly dependant on how well they emulate the human response that they are intended to represent (Crandall et al., 2009). Thus, it is not only imperative to accurately characterize human kinematic response and but also to validate the tools with which we measure such responses.

This study provides necessary assessment and validation of an innovative methodology for measuring anatomical kinematics during impact loading. The results of the tests presented here demonstrate the fundamental effectiveness of the rigid-body-motion analysis to predict the trajectories of anatomical structures within the body which are not directly visible or accessible for measurement. Additionally, the test results provide the quantified uncertainty magnitudes associated with the three major contributors for the overall uncertainty occurring in anatomical kinematic results for the impact loading environment. These contributors are 1) single target position error 2) propagation of the single target position error to the anatomical frame through coordinate transformation and 3) compliance in the assumed rigid connection between the visible target cluster and the underlying bone.

Single target data quality

The results of the single target data quality assessment (Test 001) demonstrate robust performance of the OSS to track the position of individual targets throughout the duration of a high-rate dynamic event. This is indicated by the average values of δ_i and Δ_{Diag} which were limited to a range from 0.2 mm to 0.5 mm (Figure 11). While peak deviations were as great as 1.1 mm, the S.D. of 0.1 mm indicates the majority of the deviation distribution is substantially < 1.0 mm. This finding of limited single target position error is substantiated by the fact that independent parameters (δ_i and Δ_{Diag}) to quantifying this error yielded similar results (Figure 11). The low values of δ_i indicate only minimal adjustments are required to optimally fit the digital representation to the collected single target position data at each time step (Arun et al., 1987, Beldpans et al., 1988, Magnani et al., 1993, Soderkvist and Wedin, 1993, Wang et al., 1993, Cappello et al., 1994, Challis, 1995, Cappello et al., 1996, and Cappozzo et al., 1997). This is substantiated by the correspondingly low Δ_{Diag} values indicating minimal optical distortion of the cluster during the dynamic event. A number of studies in the literature have been devoted to quantifying performance of commercially available OSSs (Ehara et al. 1995, Ehara et al. 1997, Klein et al. 1995, Linden et al., 1992, Haggard et al., 1990, Thornton et al. 1998, and Richards, 1999). While single target error for the current study is at the low end of the reported range in the literature, it should be noted that current OSS technology is utilized for the current study. Furthermore, the cluster was tracked under qualitatively “good” conditions for which all targets were visible to more than two cameras at all times during the dynamic event. This finding of such modest distortion magnitude under dynamic conditions, however, is particularly important to the application of the presented methodology. The reason being that single target position error associated with the OSS is unavoidably propagated (and likely amplified) to the anatomical location through the process of coordinate transformation (Purtsezov et al., 2010).

Effectiveness of rigid body motion analysis

Since the anatomical structures (i.e. bones) most useful for kinematic measurement are within the body, and not visible for measurement, the motion of the attached cluster must be transformed to the underlying anatomical structure to provide the desired trajectory (refer to Appendix). The accuracy of the resulting trajectory will depend on the quality of the collected cluster data, the distance between the cluster and underlying bony structure, and also the distance between individual targets on the cluster (Cappozzo et al., 1997 and Purtsezov et al. 2010). The feasibility of the presented methodology is decided by whether or not adequate performance can be achieved using cluster dimensions limited by spatial constraints for placement on the body during tests involving impacts. Using cluster and hardware dimensions representative of those used in actual PMHS sled tests (Shaw et al., 2009), the dynamic evaluation (Test 001) with the composite illustrates the fundamental ability of the rigid body motion analysis to successfully predict the directly measured anatomical trajectory. Figure 12 indicates good qualitative correlation in which the "rib" and "transformed" trajectories are nearly coincident. Quantitative assessment reveals that the peak value of deviation, Δ_{Trans}, between trajectories was 4.3 mm. While this value is small relative to the peak resultant displacement on the trajectory, it clearly demonstrates the tendency of the transformation process to amplify the modest single target position error, which was < 0.5 mm on average across parameters δ_i and Δ_{Diag}. Such amplification of OSS error is an unavoidable consequence of coordinate transformation. While the results of the evaluation test generally indicate excellent performance of the rigid body motion analysis, the demonstrated sensitivity to even low levels of intrinsic OSS error highlights the necessity of ensuring that the highest OSS single target data quality be obtained.

Hardware compliance

At a given anatomical location the visible target cluster is supported by stiff, light-weight hardware that is securely attached to the underlying bone. This supporting hardware experiences inertial loading during the test which causes bending and/or movement of the hardware relative to the bone. This compliance is not accounted for in the rigid-body-motion analysis which assumes the connection between the cluster and bone to be completely rigid, however, some hardware compliance does inevitably exist. The results of Tests 002 - 007 quantify the effects of such compliance on the accuracy of anatomical kinematic results for a range of hardware configurations typical of those currently used in PMHS sled tests. Figure 13 (Tests 002-007) provides a summary of the deviations, Δ_{Trans} , resulting from compliance in the connection between the cluster and the underlying bone during the compliance assessment tests. For these tests (Tests 002-007) peak values for Δ_{Trans} ranged from 0.9 mm to 1.7 mm. The conducted tests explored the effects of the most extreme conditions of inertial loading and movement of the hardware relative to the bone which were believed to be achievable during actual PMHS impact tests. Thus, based on these results, a reasonable upper limit for Δ_{Trans} , attributable exclusively to hardware compliance, is 2 mm.

Interpretation relative to anatomical kinematics

The results of these seven reported tests provide a practical assessment of the general magnitude of uncertainty associated with anatomical kinematic results obtained using the presented methodology. The overall uncertainty, specific to the utilized hardware, depends on a combination of the factors explored in these seven reported tests. Based on the results, the most conservative estimate is to combine the observed peak values of Δ_{Trans} occurring from both transformational and hardware compliance effects, or 4.3 mm + 2.0 mm = 6.3 mm. This uncertainty estimate is based on peak values, so a corresponding 1 S.D. of uncertainty would be 6.3 mm / 1.41 = 4.5 mm using the relation reported by Purtsezov et al. (2010). Figure 15 illustrates the "transformed" trajectories including +/- 1 S.D. of uncertainty along the X, Y, and Z axes. This is again the most conservative approach and is warranted since the data does not indicate a directional apportioning of the total uncertainty across the global X, Y, and Z axes. While the quantified level of anatomical uncertainty is substantially greater than that associated directly with the OSS, it is not unreasonable for most kinematic measurement applications where it is necessary to measure the motion of the anatomical structure, such as for impact loading. Given that the presented methodology provides the ability to track the motion of the actual anatomical structures, the anatomical uncertainty quantified here is likely small in comparison to conventional methods that only approximate anatomical motion using an external representation for which just skin artifact alone can be substantially greater even for non-impact conditions (Cappozzo et al., 1996, Manal et al., 2000, and Riemer et al. 2008).

While the results of this study demonstrate the fundamental feasibility of the presented methodology, the results are based on a limited number of tests and associated hardware configurations. The study also did not consider the uncertainty of relative displacement measures between anatomical structures (Purtsezov et al., 2010).

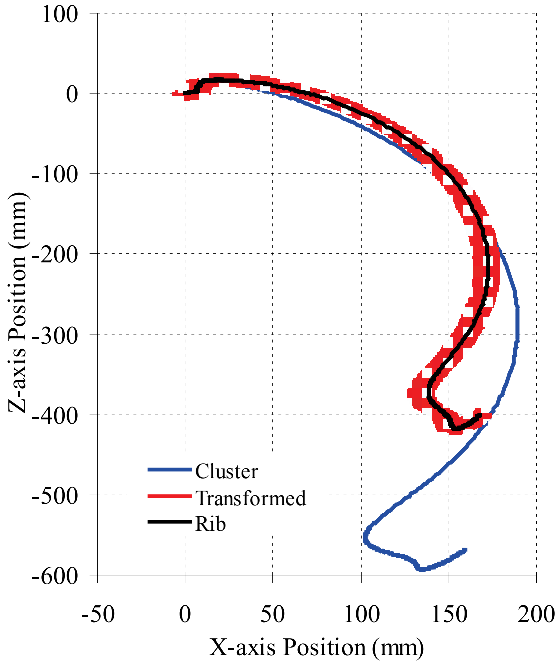

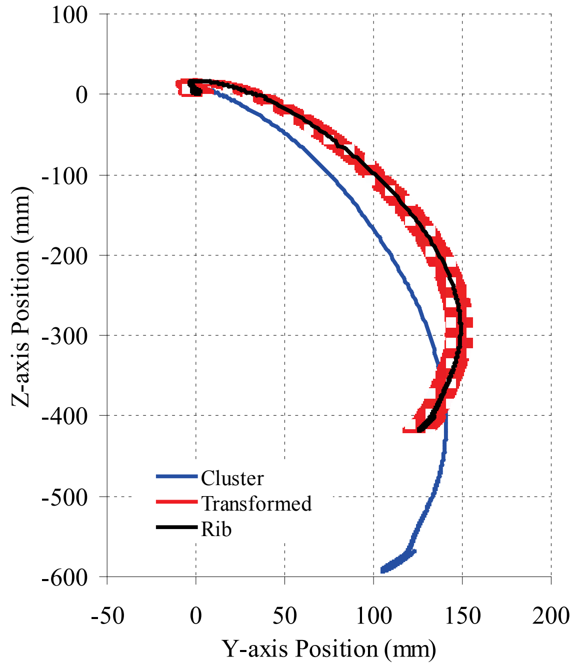

Figure 15: Transformed trajectory including +/- 1 S.D. of uncertainty along the X, Y, and Z axes.

It should be emphasized that the results provide a valuable practical assessment for the general magnitude of uncertainty in anatomical kinematic results. To be specific, however, requires an independent investigation for each anatomical measurement location taking into account the specific hardware geometry and OSS performance considerations (Purtsezov et al., 2010 and Shaw et al., 2009). Thus, providing a single uncertainty value applicable to wide range of PMHS test conditions is not possible. The presented tests were, however, designed to represent the most challenging conditions encountered during impact loading with good cluster visibility. Thus, the obtained results do provide a reasonable upper uncertainty bound for anatomical kinematics in the global reference frame when good cluster visibility is achievable. The results soundly demonstrate the feasibility of the presented methodology for measuring anatomical kinematics during impacts. While no such method is free of error, the determined resultant uncertainty upper bound of +/- 6.3mm is substantially less than typical variations in subject impact response (Shaw et al., 2009 and Forman et al., 2006). Thus, the presented methodology has sufficient resolution to characterize the response it is intended to measure and represents a valuable tool for the injury biomechanics researchers.

CONCLUSION

This study presents a necessary validation of an innovative methodology for measuring anatomical kinematics during impact loading. Specifically, the results confirm the fundamental ability of rigid-body motion analysis to use remotely measured target data, external to the body, to determine motions of underlying structures within the body. In addition to validating the fundamental methodology, the study comprehensively quantifies the magnitude of overall uncertainty in the final kinematic results, by accounting for the individual uncertainty contributions associated with the OSS, rigid-body motion analysis, and compliance of the hardware attaching visible target clusters to the underlying bone.

REFERENCES

Arun, K. Huang, T. and Blostein, S. D. (1987) Least-squares fitting of two 3-d point sets. IEEE Trans. Pattern Anal. Machine Intell., vol. PAMI-9, no. 5, pp. 698-700.

Bate, R.R., Mueller, D.D., White, J.E., (1971). Fundamentals of astrodynamics. New York: Dover Publications.

Borghese, NA. Cerveri, P. and Rigiroli, P. (2001) A fast method for calibrating video-based motion analysers using only a rigid bar. Med Biol Eng Comput, 39(1), 76-81.

Cappello, A. La Palombara, P. F. and Leardini, A. (1996) Optimization and smoothing techniques in movement analysis. Int. J. Biomed. Comput, 41(3), 137-151.

Cappello, A. Leardini, A. Catani, F. and La Palombara, P. F. (1994) Selection and validation of skin array technical references based on optimal rigid model estimation. in Proc. 3rd Int. Symp. 3-D Analysis of Human Movement, Stockholm, Sweden, pp. 15-18.

Cappozzo A; Cappello A; DellaCroce U; Pensalfini F. (1997) Surface-Marker Cluster Design Criteria for 3D Bone Movement Reconstruction. IEEE Transactions on Biomedical Engineering, 44(12): 1165-1174.

Cappozzo A; Catani F; Croce UD; Leardini A. (1995) Position and Orientation in Space of Bones During Movement: Anatomical Frame Definition and Determination. Clin Biomech, 10(4): 171-178.

Cappozzo, A. Della Croce, U. Catani, F. Leardini, A. Fioretti, S. and Maurizi, M et al., Stereometric system accuracy tests. In: Measurement and data processing methodology in clinical movement analysis-preliminary. CAMARC II Internal Report; 1993.

Cappozzo, A. Della Croce, U. Leardini, A. and Chiari, L, Human movement analysis analysis using stereophotogrammetry. Part 1: theoretical background. Gait and Posture [in press].

Cerveri, P. Borghese, NA. and Pedotti, A. (1998) Complete calibration of a stereo photogrammetric system through control points of unknown coordinates. J Biomech, 31(10), 935-40.

Challis, J. H. (1995) An examination of procedures for determining body segment attitude and position from noisy biomechanical data. Med. Eng. Phys, 17(2), 83-90.

Challis, J. H. (1995) A procedure for determining rigid body transformation parameters. J Biomech, 6, 733-737.

Chèze, L. Fregly, B. J. and Dimnet, J. (1995) A solidification procedure to facilitate kinematic analyses based on video system data. J Biomech, 28, 879-884.

Chiari L; Della CU; Leardini A; Cappozzo A. (2005) Human Movement Analysis Using Stereophotogrammetry. Part 2: Instrumental Errors. Gait Posture, 21(2): 197-211.

Crandall, JR. (2009) Simulating the road forward: the role of computational modeling in realizing future opportunities in traffic safety. International Research Council on the Biomechanics of Impact (IRCOBI).

Della Corce, U. and Cappozzo, A. (2000). A spot-check for estimating stereophotogrammetric errors. Med Biol Eng Comput, 38, 260-6.
DeLuzio KJ; Wyss UP; Li J; Costigan PA. (1993) A Procedure to Validate Three-Dimensional Motion Assessment Systems. J Biomech, 26(6): 753-759.

Ehara, Y. Fujimoto, H. Miyazaky, S. Mochimaru, M. Tanaka, S. and Yamamoto, S. (1997) Comparison of the performance of 3-D camera systems II. Gait Posture, 3, 166-9.

Ehara Y; Fujimoto H; Miyazaki S; Tanaka S; Yamamoto S. (1995) Comparison of the Performance of 3D Camera Systems. Gait Posture, 3(3): 166-169.

Forman, JL, Lessley, DJ, Kent, RW, Bostrom, O, Pipkorn, B. (2006) Whole-body Kinematic and Dynamic Response of Restrained PMHS in Frontal Sled Tests. Stapp Car Crash Journal 50: 299-336.

Forman, JL. Lopez-Valdez, F. Lessley, DJ. Kindig, M. Kent, RW. Kuppa, S. and Bostrom, O. (2009) Rear seat occupant safety; an investigation of a progressive force-limiting, pretensioning 3-point belt system using adult PMHS in frontal sled tests. Stapp Car Crash Journal, 53, 49-74.

Haggard, P. and Wing, AM. (1990) Assessing and reporting the accuracy of position measurements made with the optical tracking systems. J Motor Behav, 2, 315-21.

Holden, JP. Selbie, S. and Stanhope, SJ. (2003) A proposed test to support the clinical movement analysis laboratory accrediation process. Gait Posture, 17, 205-13.

Klein, PJ. and DeHaven, JJ. (1995) Accuaracy of three-dimensional linear and angular estimates obtained with Ariel performance analysis system. Arch Phys Med Rehabil, 76, 183-9.

Lessley, DJ, Kent, RW, Crandall, JR, Salzar, RS, and Shaw, CG. (2009) Internal vs. External Chest Deformation Response to Shoulder Belt Loading, Part 1: Table-Top Tests. Paper 2009-01-0393, Society of Automotive Engineers.

Lessley, DJ, Salzar, RS, Crandall, JR, Kent, RW, Bass, CR, Guillemot, H, and Forman, JL. (2010) Kinematics of the Thorax under Dynamic Belt Loading. International Journal of Crashworthiness (In Press)

Linden, DWV. Carlson, SJ. and Hubbard, RL. (1992) Reproducibility and accuracy of angle measurements obtained under static conditions with the motion analysis video system. Pmhs Ther, 72, 300-5.

Lopez-Valdez, F. Kent, RW. Shaw, CG. Lessley, DJ. Tanji, H. and Higuchi, K. (2009) Optical measurement of 6-DOF kinematics of internal body structures during frontal impact restraint loading, paper 20095066, Japan Society of Automotive Engineers.

Magnani, G. Angeloni, C. Leardini, A. and Cappello, A. (1993) Optimal estimation of rigid body position and attitude from noisy marker coordinates. in Proc. 14th Congress ISB, Paris, France, 820-821.

Manal, K. McClay, I. Stanhope, S. Richards, J. and Galinat, B. (2000) Comparison of surface mounted markers and attached methods in estimating tibial rotations during walking: an in vivo study. Gait Posture, 11, 38-45.

Morris, JRW. and MacLeod, A. (1990) An investigation of the sources and characteristics of noise in a video-based kinematic measurement system. In: Models, connections with experimental apparatus and relevant DSP techniques for functional movement analysis. CAMARC II Internal Report.

Purtsezov, S. Shaw, G. Lessley, D. Crandall, J. Error estimation of sternal deflection measurement with a photogrammetric system in simulated car crashes. IEEE (manuscript in preparation)

Richards, JG. (1999) The measurement of human motion: a comparison of commercially available systems. Hum Mov Sci, 18, 589-602.
Riemer, R. Hsaio-Wecksler, E. and Zhang, X. (2008) Uncertainties in inverse dynamics solutions: A comprehensive analysis and an application to gait. Gait Posture, 27, 578-588.

Shaw, CG, Lessley, DJ, Evans, J, Crandall, JR, Shin, J, Portier, P, and Paoloni, G. (2007) Quasi-static and dynamic thoracic loading tests: cadaveric torsos. International Research Council on the Biomechanics of Impact (IRCOBI).

Shaw, CG. Parent, D. Purtsezov, S. Lessley, DJ. Shin, J. and Crandall, J. (2009) Impact response of restrained PMHS in frontal sled tests: skeletal deformation patterns under seat belt loading. Stapp Car Crash Journal, 53, 1-48.

Söderkvist, I. and Wedin, P. A. (1993) Determining the movements of the skeleton using well-configured markers. J Biomech, 12, 1473-1477.

Thornton MJ; Morrissey MC; Coutts FJ. (1998) Some Effects of Camera Placement on the Accuracy of the Kinemetrix Three-Dimensional Motion Analysis System. Clinical Biomechanics, 13(6): 452-454.

Veldpaus FE; Woltring HJ; Dortmans LJMG. (1988) A Least-Squares Algorithm for the Equiform Transformation From Spatial Marker Co-Ordinates. J Biomech, 21(1): 45-54.

Wang, X. Rezgui, M. A. and Verriest, J. P. (1993) Using the polar decomposition theorem to determine the rotation matrix from noisy landmark measurements in the study of human joint kinematics. in Proc. 2nd Int. Symp. 3-D Analysis of Human Movement, Poitiers, France, 53-56.

Zhuang, HQ (1995). A self-calibration approach to extrinsic parameter estimation of stereo cameras. Rob Autonom Syst, 15, 189-97.

APPENDIX

(Adapted from Shaw et al., 2009)

Coordinate transformation was an integral part of the rigid body motion analysis since the focus of interest (i.e. the bone) was not directly visible to the video-based optoelectronic stereophotogrammetric system (OSS). Determining the bone trajectory required the cluster trajectory to be “transformed” to the bone using a series of coordinate transformations. Before providing the specific details concerning the transformation used for the presented tests, a brief review of coordinate transformations is provided.

As described by Bate et al. (1971), a vector may be expressed in any number of rectangular coordinate systems, where each coordinate system is defined first, by specifying the location of its origin, followed by specifying the direction of the three mutually orthogonal axes defined by three corresponding unit vectors. A coordinate transformation does not alter the vector, but instead alters the vector components. This allows the vector to be transformed from one reference frame to another which is the equivalent to changing the perspective of expressing the vector from one frame of reference to another.

Figure A1 illustrates three arbitrary rectangular coordinate systems; $\mathbf{X_1Y_1Z_1}$, $\mathbf{X_2Y_2Z_2}$, and $\mathbf{X_3Y_3Z_3}$ corresponding to coordinate systems 1, 2, and 3 respectively. The axes of each coordinate system are defined by three mutually orthogonal unit vectors; $\boldsymbol{i}_1$, $\boldsymbol{j}_1$, and $\boldsymbol{k}_1$, for the coordinate system #1; $\boldsymbol{i}_2$, $\boldsymbol{j}_2$, and $\boldsymbol{k}_2$ for coordinate system #2, and $\mathbf{i}_3$, $\mathbf{j}_3$, and $\mathbf{k}_3$ for coordinate system #3. An arbitrary point in space, P, is expressed in each of the three coordinate systems using a position vector, $\boldsymbol{P}_{P1}$, $\boldsymbol{P}_{P2}$, and $\boldsymbol{P}_{P3}$, from the origin of the respective coordinate system to the position of point, P. The position vectors’ components correspond to the Cartesian coordinates of the point P in each of the three coordinate systems. Representing point P in homogenous coordinates (i.e. (X_1, Y_1, Z_1, 1) allows the relationship between position vectors to be quantified using Equation 1.

Referring to Figure A1, the components of the position vector, $\boldsymbol{P}_{P1}$, from the origin of system #1 to point P, is given by multiplication of a square [4 X 4] matrix and a [4 X 1] column matrix. The [4 X 1] column matrix represents the coordinates of the position vector, $\boldsymbol{P}_{P2}$, from the origin of system #2 to point P. The square [4 X 4] matrix is referred to as a transformation matrix. The definition of the elements of the transformation matrix are provided in Equation 1, where tij is the dot product of the ith unit vector in coordinate system #2 and the jth unit vector in coordinate system #1. Px, Py, and Pz are the elements of the vector, $\boldsymbol{P}_{21}$, defining the position of the origin of coordinate system #2 relative to coordinate system #1. The transformation matrix is referred to as, $T_{2/1}$, meaning the transformation from coordinate system of #2 to coordinate system #1.

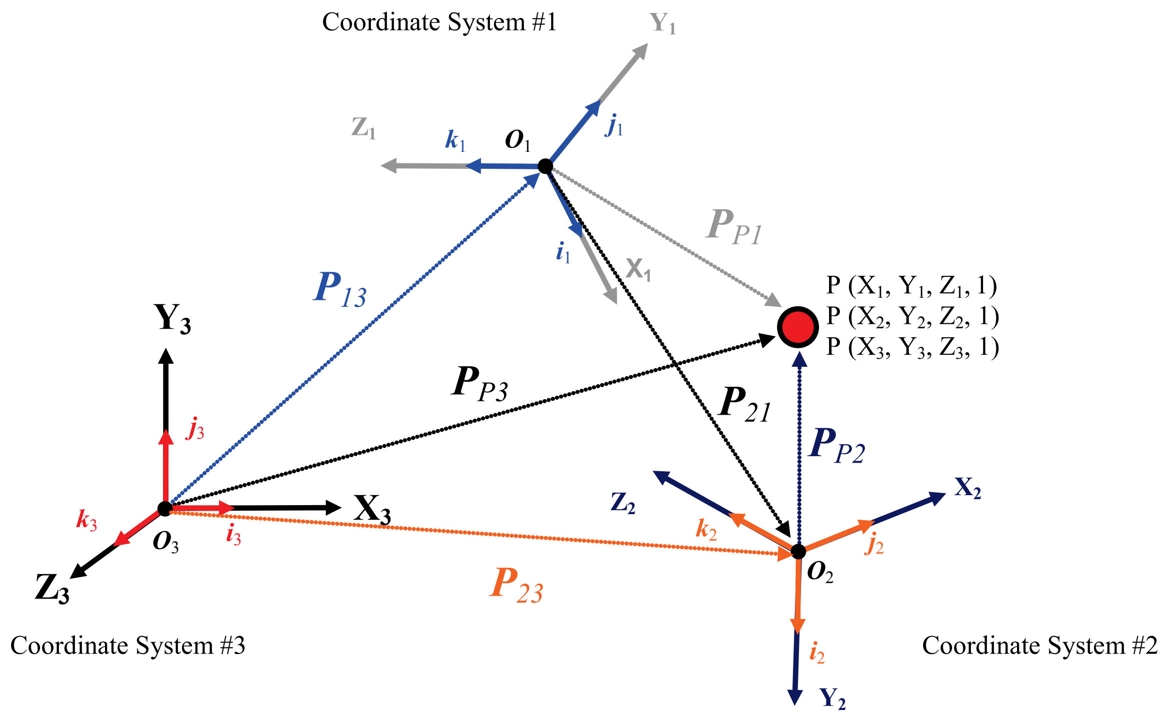

Figure A1: Relationship between global and local coordinate systems.

$$\begin{bmatrix} X_1 \\ Y_1 \\ Z_1 \\ 1 \end{bmatrix} = \begin{bmatrix} t_{11} & t_{12} & t_{13} & P_x \\ t_{21} & t_{22} & t_{23} & P_y \\ t_{31} & t_{32} & t_{33} & P_z \\ 0 & 0 & 0 & 1 \end{bmatrix} * \begin{bmatrix} X_2 \\ Y_2 \\ Z_3 \\ 1 \end{bmatrix} = \begin{bmatrix} (\vec{i}_2 \circ \vec{i}_1) & (\vec{j}_2 \circ \vec{i}_1) & (\vec{k}_2 \circ \vec{i}_1) & (\vec{P}_{21} \circ \vec{i}_1) \\ (\vec{i}_2 \circ \vec{j}_1) & (\vec{j}_2 \circ \vec{j}_1) & (\vec{k}_2 \circ \vec{j}_1) & (\vec{P}_{21} \circ \vec{j}_1) \\ (\vec{i}_2 \circ \vec{k}_1) & (\vec{j}_2 \circ \vec{k}_1) & (\vec{k}_2 \circ \vec{k}_1) & (\vec{P}_{21} \circ \vec{k}_1) \\ 0 & 0 & 0 & 1 \end{bmatrix} * \begin{bmatrix} X_2 \\ Y_2 \\ Z_2 \\ 1 \end{bmatrix} \Rightarrow \vec{P}_{P1} = T_{2/1} * \vec{P}_{P2} \qquad [1]$$

The relationship described above in Equation 1 can be used to relate the transformation matrices between various pairs coordinate systems. This is expressed in Equations 2-6 below. Equations 2 and 3 relate the transformations between the position vectors of coordinate systems #1 and #2 with the position vector of coordinate system #3. Combining Equations 2 and 3 yields Equation 4. Finally, combining Equations 4 and 1, relates the transformation matrices occurring between pairs of coordinate systems. Importantly, Equation 5 can be used to obtain a transformation matrix whenever two coordinate systems are defined relative to a common third coordinate system.

$$\vec{P}_{P3} = T_{1/3} * \vec{P}_{P1} \qquad [2]$$

$$\vec{P}_{P3} = T_{2/3} * \vec{P}_{P2} \qquad [3]$$

$$T_{1/3} * \vec{P}_{P1} = T_{2/3} * \vec{P}_{P2} \qquad [4]$$

$$T_{2/1} = [T_{1/3}]^{-1} * T_{2/3} \Rightarrow T_{2/3} = T_{1/3} * T_{2/1}$$
[5]

Obtaining the anatomical trajectories from marker-cluster trajectories

Using the method described above, a number of transformation matrices were developed to relate the four rigid body coordinate systems to each other and also to the OSS coordinate system. The OSS coordinate system will be referred to as the global coordinate system. Figure E2 illustrates the five coordinate systems associated with each anatomical measurement location. These are the marker (M), plate (P), mount (Mo), bone (B), and global (G) coordinate system.

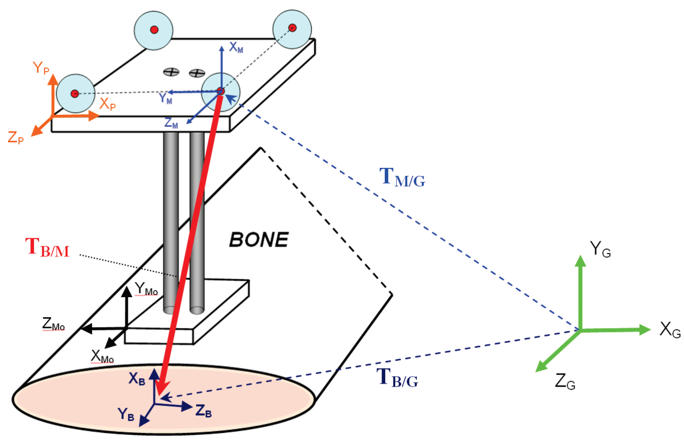

Figure A2: Process of obtaining 6DOF kinematics of an anatomical landmark relative to the global coordinate system using coordinate transformation. The transformation matrices $T_{M/G}$, $T_{B/M}$, and $T_{B/G}$ are described above.

Equations 6 – 9 relate the transformation matrices corresponding to selected pairs of coordinate systems. $T_{P/M}$ defines the relationship between the position vectors of point in expressed in the marker and plate coordinate systems and was obtained using data collected from the FARO arm. According to Equation 1, $T_{Mo/P}$ defines the relationship between the position vectors of point in expressed in the mount and plate coordinate systems and was obtained using geometry from the manufacturing schematics of the hardware. $T_{Mo/M}$ defines the relationship between the position vectors of point in expressed in the mount and marker coordinate systems and was obtained using Equation 6. $T_{B/Mo}$ defines the relationship between the position vectors of point in expressed in the bone and mount coordinate systems and was obtained using the pretest CT data. $T_{B/M}$ defines the relationship between the position vectors of point in expressed in the bone and marker coordinate systems and was obtained using Equation 7. $T_{M/G}$ defines the relationship between the position vectors of point in expressed in the marker and global coordinate systems. $T_{M/G}(t)$ varied with time, and was result of the smoothed marker-cluster trajectories that were initially smoothed via a rigidity constraint using the least squares pose (LSP) estimator as performed by Cappozzo et al., (1997). $T_{B/G}(t)$ defines the relationship between the position vectors of point in expressed in the bone and global coordinate systems for a given time, t, and was obtained using Equation 8. Equation 9 (based on Equation 1) is used to provide the Cartesian coordinates of the bone coordinate system origin for the time interval over which $T_{B/G}(t)$ is defined. $T_{B2/B1}$ defines the relationship between the position vectors of point in expressed in two different bone coordinate systems and is obtained using Equation 10. Equation 11 can be used to determine the position of the origin of bone coordinate system #2 relative to the origin of bone coordinate system #1 at a give time, t.

$$[T_{Mo/M}] = [T_{P/M}] * [T_{Mo/P}] \quad [6]$$

$$[T_{B/M}] = [T_{Mo/M}] * [T_{B/Mo}] \quad [7]$$

$$[T_{B/G}(t)] = [T_{M/G}(t)] * [T_{B/M}] \quad [8]$$

$$\begin{bmatrix} X_G(t) \\ Y_G(t) \\ Z_G(t) \\ 1 \end{bmatrix} = \left[T_{B/G}(t)\right] * \begin{bmatrix} 0 \\ 0 \\ 0 \\ 1 \end{bmatrix} \qquad [9]$$

$$\left[T_{B2/B1}(t)\right] = \left[T_{B1/G}(t)\right]^{-1} * \left[T_{B2/G}(t)\right] \qquad [10]$$

$$\begin{bmatrix} X_{21}(t) \\ Y_{21}(t) \\ Z_{21}(t) \\ 1 \end{bmatrix} = \left[T_{B2/B1}(t)\right] * \begin{bmatrix} 0 \\ 0 \\ 0 \\ 1 \end{bmatrix} \qquad [11]$$